

RSC Advances



This is an *Accepted Manuscript*, which has been through the Royal Society of Chemistry peer review process and has been accepted for publication.

Accepted Manuscripts are published online shortly after acceptance, before technical editing, formatting and proof reading. Using this free service, authors can make their results available to the community, in citable form, before we publish the edited article. This *Accepted Manuscript* will be replaced by the edited, formatted and paginated article as soon as this is available.

You can find more information about *Accepted Manuscripts* in the [Information for Authors](#).

Please note that technical editing may introduce minor changes to the text and/or graphics, which may alter content. The journal's standard [Terms & Conditions](#) and the [Ethical guidelines](#) still apply. In no event shall the Royal Society of Chemistry be held responsible for any errors or omissions in this *Accepted Manuscript* or any consequences arising from the use of any information it contains.

DFT insights into cycloisomerization of ω -alkynylfuran catalyzed by planar gold clusters: mechanism and selectivity, as compared to Au(I)-catalysis

Received 00th January 20xx,
Accepted 00th January 20xx

DOI: 10.1039/x0xx00000x

www.rsc.org/

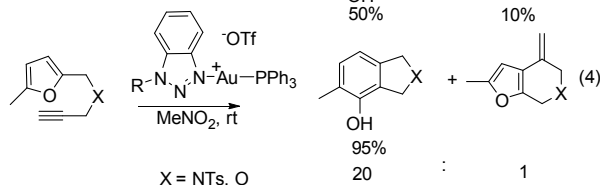
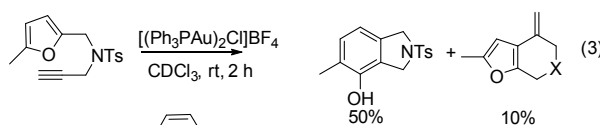
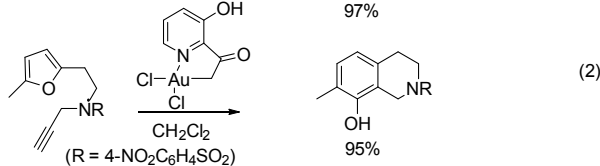
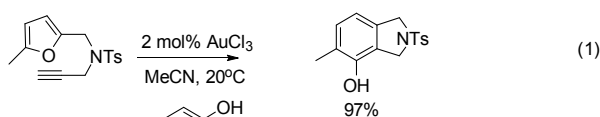
Miao Yang,^{a,b} Zhongzhu Chen,^b Yafei Luo,^b Jin Zhang,^b Dianyong Tang,^{b*} Rongxin He,^a Wei Shen^a and Ming Li^{a*}

A detailed reaction mechanism of the triatomic gold cluster-catalyzed cycloisomerization of ω -alkynylfuran was systematically investigated via the density functional theory at the TPSSh/def2-TZVP level. The computational results indicated that the 5-exo Friedel-Crafts-type mechanism is the most favorable mechanism to form the phenol derivatives. The strong interaction between the gold and vinyl fragment in the Friedel-Crafts adduct is essential for the priority of the 5-exo Friedel-Crafts-type mechanism. Then, the 5-exo Friedel-Crafts-type mechanism on the various planar gold clusters (Au₄–10) was studied to clarify the size-effects of the planar gold clusters catalyzed ω -alkynylfuran cycloisomerization. The appropriate interactions between the alkyne group in substrate and gold clusters play a key role for the 5-exo cyclization step. The energy barriers of the ring-closure of the dienone carbene-gold intermediate step show an interesting “odd-even” behavior respective to the number of gold atoms. The Au₃ and Au₄ clusters are the most active catalysts for the ω -alkynylfuran cycloisomerization to phenol derivative. We also found that the active catalyst of the ω -alkynylfuran cycloisomerization catalyzed by the gold(I) complexes should be the gold(0) complexes of the in situ generation. The catalytic activity of the gold(0) complex is comparable with that of the planar gold clusters. These findings may guide the rational design of highly active gold catalysts for the ω -alkynylfuran cycloisomerization to phenol derivatives.

Introduction

The gold-catalyzed phenol synthesis is an isomerization reaction that transforms a ω -alkynylfuran to an annellated phenol via the cleavage of four bonds and the formation of four new bonds. It is an intramolecular reaction of the alkyne-gold complex with the furan ring. After the first report by the Hashmi group in 2000 (Scheme 1),¹ many reports about the phenol synthesis from the ω -alkynylfuran isomerization have emerged over the past few decades (Scheme 1).^{2–14} Pt(II), Pd(II), Ir(I), and Rh(I) were also found to catalyze the intramolecular reactions of alkynes with arenes and furans (Scheme 2).^{2,13,14} Still, gold complexes are clearly more active than other metals, display effective chemoselectivity and high synthetic efficiency in the cycloisomerization of ω -alkynylfurans, and yield no significant side products under mild conditions (Scheme 1).^{2,3,9} The cationic binuclear gold(I) complex [(Ph₃PAu)₂Cl]BF₄ could catalyze

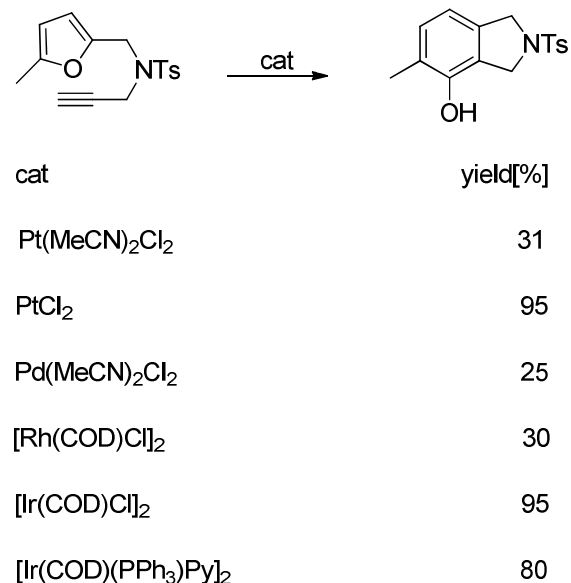
the cyclization of ω -alkynylfurans to the main product phenols with the annellated furans as the side-products.⁴ The 1,2,3-triazole was used as a special “X-factor” (as a ligand for [AuPPh₃]⁺ coordination forming a [Ph₃P-Au-triazole]⁺ complex) to stabilize the gold catalyst and obtain excellent yields and chemoselectivity by Shi group.⁹ The X-factor, which was developed by using the 1,2,3-triazole as a



^a School of Chemistry and Chemical Engineering, Southwest University, Chongqing 400715, P. R. China. Tel: +86-23-68366688; E-mail: liming@swu.edu.cn

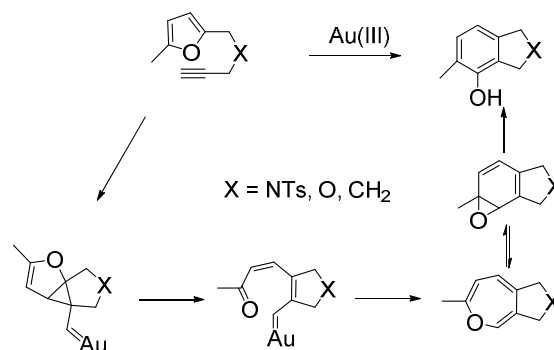
^b Research Institute for New Materials Technology and Chongqing Key Laboratory of Environmental Materials and Remediation Technologies, Chongqing University of Arts and Sciences, Chongqing, 402160, P. R. China. Tel: +86-23-61162836; E-mail: tangdy2008@163.com

Electronic Supplementary Information (ESI) available: Figs. S1–S15, Table S1–S9, details of the energy decomposition analysis, and the cartesian coordinates, single point electronic energies (in the gas phase and acetonitrile), zero-point, and free energy correction for all of the stationary points and imaginary frequencies of transition structures. See DOI: 10.1039/x0xx00000x

Scheme 1 Gold-catalyzed cycloisomerizations of ω -alkynylfurans.Scheme 2. Different transition metal complex-catalyzed- ω -alkynylfurans cycloisomerizations.

coordination factor to stabilize the catalyst, could be regarded as an alternative strategy, instead of tuning the phosphorus ligands.⁹ The Hashmi group also found that the mononuclear NAC-gold(I) and phosphite-gold(I) catalysts are highly active for the cyclization of ω -alkynylfurans. Turn-over numbers up to 37,000 for the cyclization of ω -alkynylfurans were obtained.^{11,12} Gold nanoparticles supported on nanocrystalline CeO₂ could also catalyze the cycloisomerization of ω -alkynylfurans to phenols.¹⁵

Remarkable works have also been performed regarding the elucidation of this mechanism including the successful isolation of several key intermediates, that is, the arene oxide and oxepine.^{7,16} The breakage and formation of four bonds during this reaction is clearly not an elementary reaction. Because the rate-limiting step possesses lowest reaction rate in the overall reactions (reaction kinetic theory), the reaction intermediate of this step should be opulent and be detectable by the NMR, IR etc. Therefore, based on the kinetic theory and ¹H NMR spectroscopy, Hashmi et al concluded that the failure to detect intermediates with AuCl₃ simply means that the first step was the rate-limiting step.¹⁷ Hashmi et al. demonstrated that the oxygen atom is transferred intramolecularly during the reaction.² The Hashmi group showed that the reaction does not proceed via an alkynyl or a vinylidene complex because a primary kinetic isotope effect was not observed with a substrate deuterated at the alkyne.¹⁶ The Echavarren group found that the intramolecular reaction of furans with alkynes catalyzed by PtCl₂ is mechanistically related to that of enyne in polar solvents.^{13,14} The PtCl₂-catalyzed reaction is initiated by the nucleophilic attack of the furan on a (η^2 -alkyne)Pt(II) complex to form a cyclopropyl platinum



Scheme 3. Proposed mechanism for the gold-catalyzed phenol synthesis.

carbene via density functional theory calculations. According to ¹⁸O labeling experiments,¹ substrate deuteration studies,¹⁶ and *in situ* NMR spectroscopy,^{7,17} Hashmi et al. proposed a mechanism for the Au(III)-catalyzed phenol synthesis reaction shown in Scheme 3. The reaction kinetic studies provided strong evidence that the actual Au(I) catalyst was likely the Ph₃PAu⁺ complex, which was under equilibrium with precatalyst [Ph₃P-Au-triazole]⁺ as shown by the Shi group.⁹ Recently, Oliver-Meseguer et al. used matrix-assisted laser desorption/ionization–time-of-flight mass spectrometry (MALDI-TOF) and ultraviolet-visible (UV-vis) spectroscopy to report that very small (3~6 atoms) gold clusters generated *in situ* from gold salts, complexes, and/or nanoparticles can catalyze this reaction.¹⁸ Moreover, the small gold clusters (only 3 to 10) can be formed from different Au(I) and Au(III) salts or gold complexes during a catalytic process in solution at room temperature in some cases; they can efficiently activate the C-C triple bond of alkynes.¹⁹⁻²¹ For instance, the ester-assisted hydration of alkynes catalyzed by small gold clusters could yield an unprecedented ~10⁷ turnover number (TON).¹⁹ In addition, the ligand can play some significant roles in the activity of the catalyst, including two main aspects. One respect is the gold catalysts in different oxide state and ligands can cause different product distributions. As shown in Scheme 1, gold catalysts in different oxidation states and ligand produce different product distributions.¹⁻¹² Another aspect is the ligand can exert a straightforward influence on the formation and stability of the small clusters, which has been demonstrated by kinetic and spectroscopic studies.¹⁸⁻²¹ Distinctly, the formations of gold clusters and the catalytic activity inevitably depend on the chemical nature of ligands and counter anions in the complexes, which is reported by Corma group.²¹ Meanwhile, the gold complexes with different ligands can cause obviously catalytic activity, which can be found in many previous studies.^{1-12,21}

The previous experimental studies also showed that the formation of phenol should proceed via arene oxide or oxepine intermediate because of their capture in a Diels-Alder reaction with dienophiles and detection with *in situ* NMR spectroscopy.^{7,17} However, the formation of arene oxide or oxepine intermediate from reactants under experimental conditions remains unclear. Other questions include: Which gold species is the active catalyst in these reactions? How do we control the product selectivity via

active gold species? To answer some of these questions, the planar gold clusters were chosen as the active catalysts to investigate the detailed mechanism of the ω -alkynylfurans cycloisomerization. The planar gold clusters were assumed to be the active catalyst of the ω -alkynylfuran cycloisomerization catalyzed by Au(I) and Au(III) complexes in some cases.^{18,21} In our previous papers, the alkyne activation reactions including the cycloisomerization of 1,6-enyne and the cycloisomerization/oxidative dimerization of phenyl propargyl ether catalyzed by the Au₃₈ cluster were investigated.^{22,23} The present theoretical mechanistic investigations are aimed at extending the understanding of ω -alkynylfuran cycloisomerization catalyzed by the planar gold clusters by elucidating the following intriguing, but not yet firmly resolved aspects: (1) Which is the preferred mechanism for the ω -alkynylfuran cycloisomerization catalyzed by the planar gold clusters? (2) What is the source of product selectivity? (3) How does the size of the planar gold clusters affect the catalytic activity? (4) Which factor controls the catalytic activity of the planar gold clusters? (5) Which is true active catalyst for the ω -alkynylfurans cycloisomerization catalyzed by the gold(I) complexes? It should be noted that our efforts focused on the mechanism of ω -alkynylfuran cycloisomerization catalyzed by the planar gold clusters and AuPPh₃⁺ complex. The truly active catalyst and mechanism of the ω -alkynylfuran cycloisomerization catalyzed by the different oxidation state gold species (such as AuCl, AuCl₃, Au(I) complexes, and Au/CeO₂) will be investigated in the future.

Computational details

The mechanism was investigated via density functional theory (DFT) using the TPSSH functional^{24,25} with the def2-TZVP²⁶ basis sets as implemented in Gaussian 09 package,²⁷ which was used in the geometric optimizations of intermediates (IMs) and transition states (TSs). To check the IMs and TSs structures, vibrational frequency calculations at the same level of theory were performed. Intrinsic reaction coordinates (IRC)^{28,29} were performed to confirm the transition states connecting with the corresponding reactant and product intermediates. According to reaction conditions, the solvent effect of acetonitrile ($\epsilon = 37.5$) was evaluated using the SMD model (where "SM" and "D" stand for solvation model and density, respectively).³⁰ Natural charges were calculated via natural population analysis at the same level as that used for geometry optimization.

The adsorption energies of the gold cluster substrates are defined in Eq. 1.

$$\Delta E_{\text{ads}} = E_{\text{total}} - E_{\text{cluster}} - E_{\text{substrate}} \quad (1)$$

Where E_{total} , E_{cluster} , and $E_{\text{substrate}}$ are the total energies of the adsorbed substrate on the cluster, the bare cluster, and the substrate, respectively. The relative Gibbs free energies of stationary points at 298.15 K and 1 atm are also presented in the Figures. The adsorption energies of these clusters were only affected by the entropy effect. The activation free energies are similar to that of the energy barriers. Therefore, only the energy barriers and reaction energies were discussed unless otherwise stated.

It should be noted that that the spin-orbital coupling can play important role in the calculation of both, the atomization energies and the relative stability of the isomers of gold clusters.³¹ However, due to the large computational times, the spin-orbital coupling is not considered in the gold-catalyzed reactions, such as CO oxidation, C-C coupling reaction, water-gas shift reaction, et al.³²⁻³⁶ Similarly, the spin-orbital coupling is not considered in the current paper.

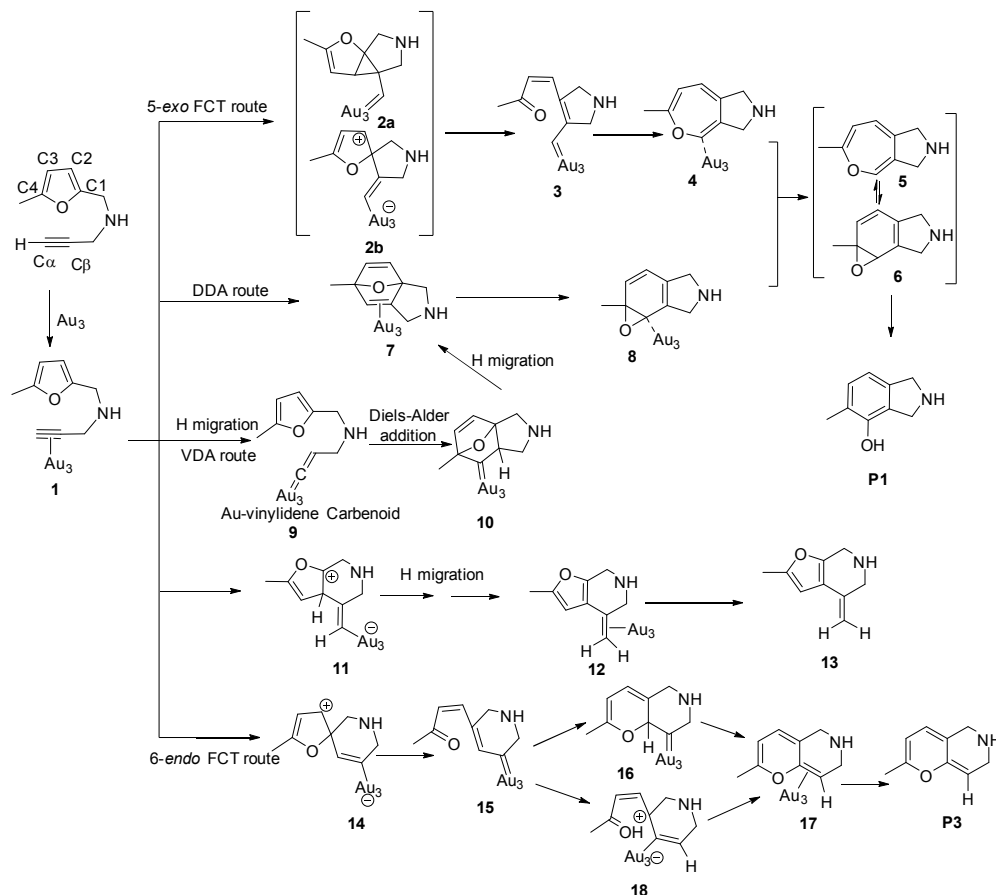
Results and discussion

It should be noted that the charge states of the gold clusters are neutral in the present study. The reasons are mainly collected as the following two points. Firstly, according to the experimental results, the detection of *in situ* UV-vis characteristic peak shows the formation of neutral Au₃ and Au₄ clusters,¹⁸⁻²¹ not the Au_n⁺ clusters. Secondly, we also calculate the reaction mechanisms via using the Au₃⁺ and Au₄⁺ clusters as the catalysts. However, the **TS2/3** and **TS3/4** could not be located with our best endeavor. The potential energy surface scan unveils that the energy is increasing for **IM2** → **IM3** and **IM3** → **IM4**. Therefore, in order to consistent with the experimental results,¹⁸⁻²¹ the Au_n⁺ clusters are not considered as the active catalysts in this manuscript.

In the present paper, the hybrid meta-GGA functional TPSSH was utilized because of the very good metal-ligand bond energies, cohesive energy of metal clusters, and structural parameters of metal clusters it is reported to provide.³⁷⁻⁴² To confirm our choice of functional and basis set, the possible structures for Au₃₋₁₀ were optimized and shown in Fig. S1. The predicted bond lengths of the Au-Au bond in Au₂ and Au₃ is 2.518 and 2.563 Å, which is in line with those at the CCSD(T)-F12a/def2-TZVP levels (2.476 and 2.519 Å), respectively.⁴³ The cohesive energies of Au₂ and Au₃ are 24.32 and 24.63 kcal/mol, which is also in agreement with the experimental results (26.82 and 29.23 kcal/mol), respectively.⁴⁴⁻⁴⁶ For the Au₃ cluster, the acute triangle structure is higher than the obtuse triangle structure about 1.67 kcal/mol, which is in line with results obtained at the various functionals and basis sets.^{31,47} As shown in Fig. S1, the stable gold clusters of each gold cluster are in line with the previous results.^{31,43, 47-49} Therefore, the functional and basis sets could produce the reliable results for the structural and properties of the gold clusters.

Mechanism for ω -alkynylfuran cycloisomerization catalyzed by Au₃ cluster.

To illustrate the catalytic behavior of planar gold clusters, the Au₃ cluster was selected as a model catalyst to simulate the detailed mechanism of the ω -alkynylfuran cycloisomerization. The Au₃ cluster was assumed to be the active catalyst of the ω -alkynylfuran cycloisomerization catalyzed by Au(I) and Au(III) complexes in some cases.¹⁸ According to the mechanism proposed by the Hashmi group,^{7,15-18} the possible pathways of the ω -alkynylfuran cycloisomerization catalyzed by Au₃ clusters were designed and



Scheme 4. The 5-*exo* Friedel–Crafts-type (FCT) route, direct Diels–Alder-type (DDA) route, and Au–vinylidene carbenoid (VDA) route to form the phenol derivative (P1), the formation of β -alkenylated furan (P2), and the 6-*endo* Friedel–Crafts-type (FCT) route toward the pyran derivative (P3).

shown in Scheme 4. The energy profiles, optimized structures, and related parameters are depicted in Figs. 1–5.

Adsorption of ω -alkynylfuran. It is well-known that the geometric structure of neutral Au_3 cluster is obtuse triangle.^{31,47,50} As shown in Fig. 1, the adsorption of the ω -alkynylfuran on the Au_3 cluster induces the structure deformation of the Au_3 cluster into acute triangle (Fig. 1). The adsorption energy of the substrate on the Au_3 cluster is -32.84 (-29.05) kcal/mol in the gas phase due to the strong σ -donation from the π orbital of the $\text{C}\equiv\text{C}$ bond as well as the partially occupied d orbital of the gold atom and the π -back-donation from the d orbital of the gold atom to the π^* orbital of the $\text{C}\equiv\text{C}$ bond. The interaction between the alkyne fragment and Au_3 is similar to that of alkyne fragments of 1,6-enyne and aryl propargyl ether with the surface gold atom of the Au_{38} clusters.^{22,23} The adsorption of substrate causes the net transfer of electron from Au_3

fragment to substrate fragment. (The natural charge on the Au_3 fragment is about 0.17 |e|). The received electron from the substrate fragment is mainly distributed on the $\text{C}\equiv\text{C}$ bond, which enhances the nucleophilicity of two carbon atoms. Hence, the adsorption of substrate favors the subsequent nucleophilic addition. At the same time, the adsorption of substrate results in the activation of $\text{C}\equiv\text{C}$ bond, which is reflected by the increasing $\text{C}\equiv\text{C}$ bond length from 1.20 Å to 1.25 Å due to the back-donation of d electrons to the π^* orbital of the $\text{C}\equiv\text{C}$ bond.

Pathways for the formation of phenol. As shown in Scheme 4, after the adsorption of substrate on Au_3 cluster, there are four possible pathways to produce phenol derivatives. The first one is 5-*exo* Friedel–Crafts-type reaction route starting from the nucleophilic

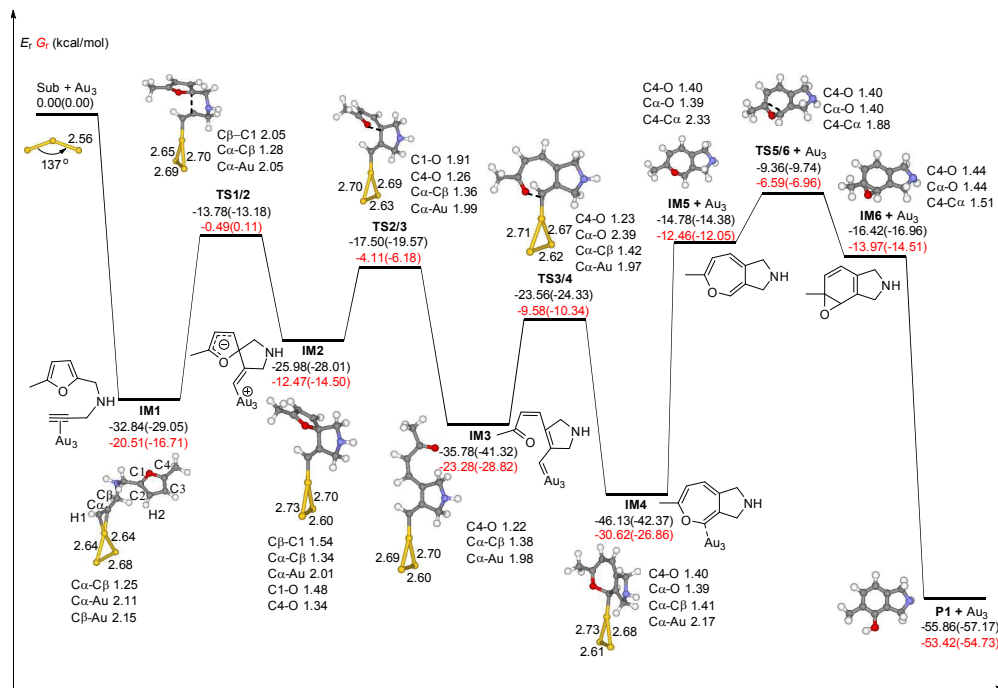


Fig. 1 The optimized structures, related parameters, potential energy profile, and relative Gibbs free energies (colored in red, 298.15 K and 1 atm) of the 5-*exo* FCT pathway to form the phenol derivative **P1** in the gas phase and acetonitrile solvent (parentheses) are shown. The bond length is in Å.

addition of a C β atom to the C1=C2 bond or C1 site of furan ring (abbreviated as 5-*exo* FCT). The second pathway is the [4+2] cycloaddition between the C \equiv C bond and the C1=C2-C3=C4 of the furan ring to produce the final product (abbreviated as DDA). The last pathway is a direct hydrogen transfer from the C α atom to the C β atom to form an Au-vinylidene carbenoid intermediate, and subsequent Diels-Alder addition of the C α -C β double bond to the furan ring (abbreviated as VDA). It is unlikely that the pathway proceeds via an alkynyl or a vinylidene complex because a primary kinetic isotope effect was not observed with a substrate deuterated at the alkyne,¹⁶ but this pathway is presented for comparison. In the following sections, the 5-*exo* FCT, DDA, and VDA pathways are discussed in further detail.

Firstly, the 5-*exo* FCT reaction route is discussed (Fig. 1). After formation of **IM1**, the nucleophilic addition of the C β atom to the C1 site of the furan ring results in a metastable spiro-intermediate **IM2** (the 5-*exo* cyclization step). Because the delocalization of the negative charge in **IM2** is not sufficient to compensate for the stability of the gold vinyl, this step is energetically unfavorable and

is endothermic by 6.86 and 1.04 kcal/mol in the gas phase and acetonitrile solvent, respectively. This step needs to overcome about 19.06 and 15.87 kcal/mol in the gas phase and acetonitrile solvent, respectively. We also considered the nucleophilic addition of C β atom to the C1-C2 bond of furan to give the gold-cyclopropylcarbene complex (**2a**, Scheme 4), but only a minimum-energy structure could be located. The transition state connecting with the **IM1** and gold-cyclopropylcarbene complex could not be located. The predicted energy of the gold-cyclopropylcarbene complex is higher than that of **IM2** by about 5 kcal/mol, which indicated that the formation of the gold-cyclopropylcarbene complex is thermodynamically unfavorable.

This point is significantly different from the PtCl₂-catalyzed intramolecular reaction of furan with alkyne in which the formation of the Pt-cyclopropylcarbene complex is thermodynamically and kinetically favorable.^{13,14} The charges on C β , C1, and C2 atoms of **IM1** are -0.10, 0.27, and -0.31 |e|, respectively, which supports the formation of the Friedel-Crafts complex **IM2**. The C1-O bond is lengthened to 1.48 Å in **IM2** indicating the activation of a C-O bond.

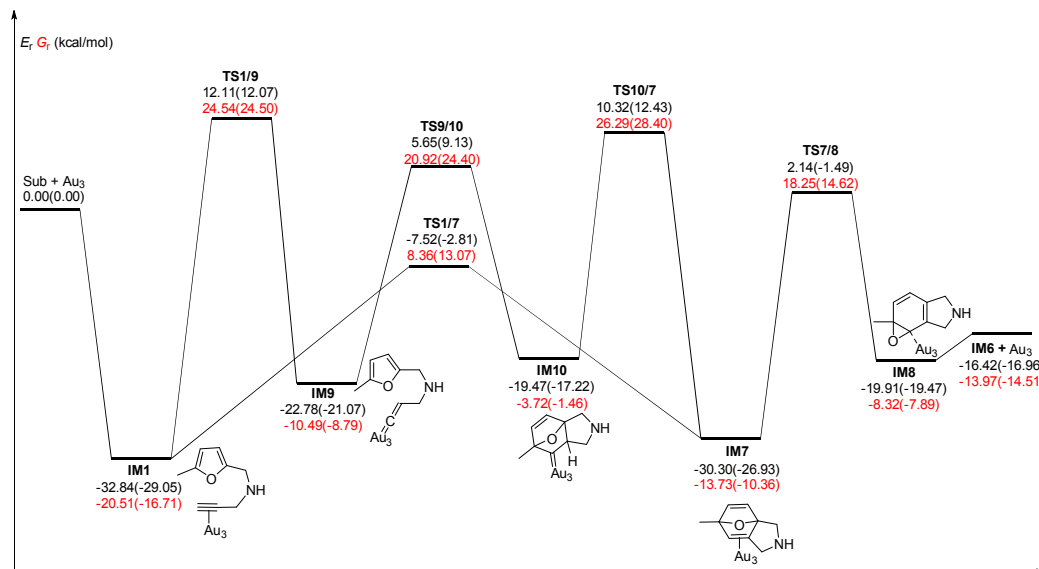


Fig. 2 Potential energy profiles and relative Gibbs free energies (colored by red, 298.15 K and 1 atm) of the DDA and VDA pathways to form phenol derivative **P1** in the gas phase and acetonitrile solvent (parentheses). The bond length is in Å.

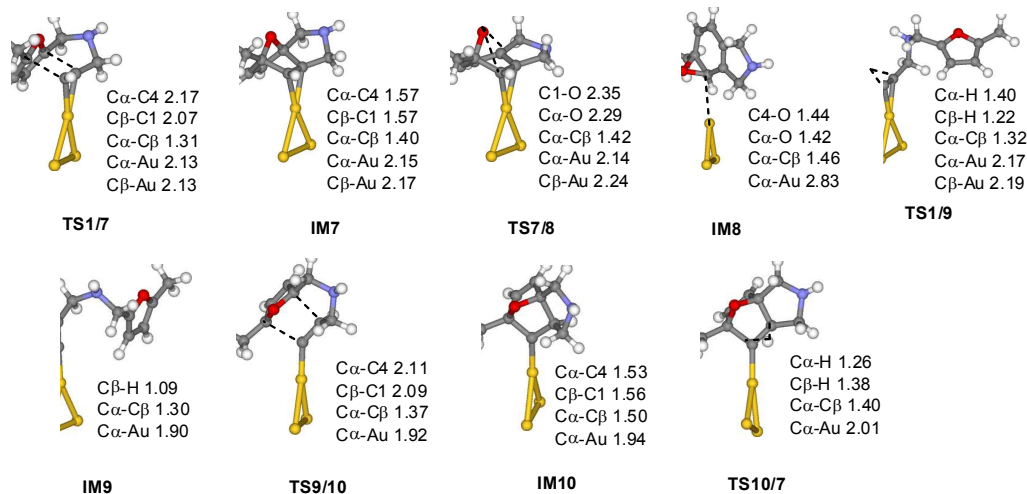


Fig. 3 The optimized structures and related parameters for DDA and VDA pathways (bond length in Å).

This activation is favorable for the following step of the C1-O bond cleavage. Subsequently, the cleavage of the C1-O bond forms a conjugate dienone carbene-gold intermediate **IM3** (the ring-opening of furan step). **IM3** should be more stable than **IM2** due to the strong delocalization of charges in **IM3**. As expected, this step is

exothermic by about 9.80 and 13.31 kcal/mol in the gas phase and acetonitrile solvent, respectively. The energy barrier of the C1-O bond cleavage is only 8.48 and 8.44 kcal/mol in the gas phase and acetonitrile solvent, respectively, because of the strong activation of the C1-O bond in **IM2**.

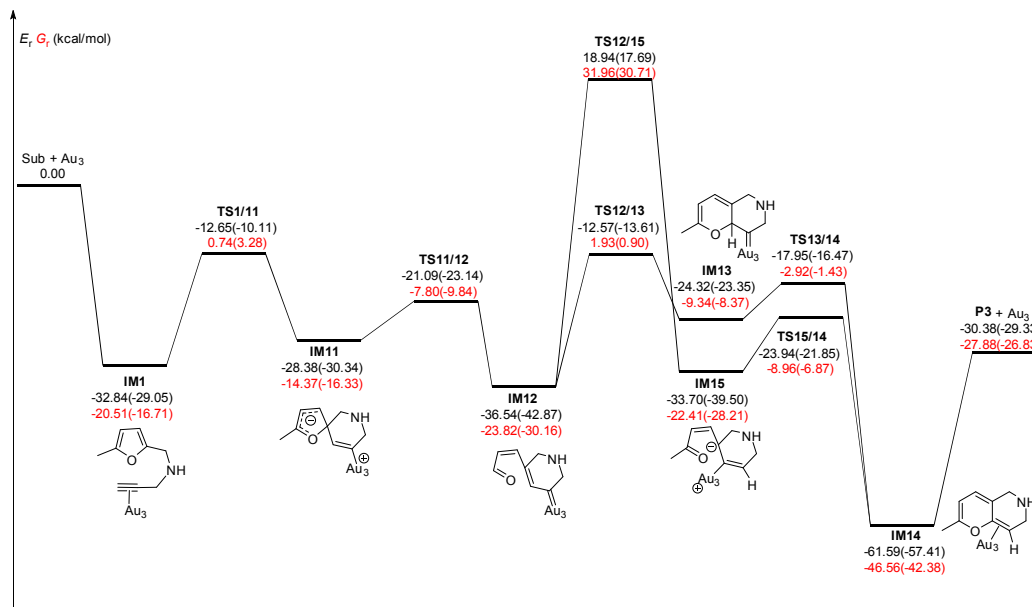


Fig. 4 Potential energy profiles and relative Gibbs free energies (colored by red, 298.15 K and 1 atm) of the 6-endo FCT pathway toward pyran derivative **P3** in the gas phase and acetonitrile solvent (parentheses).

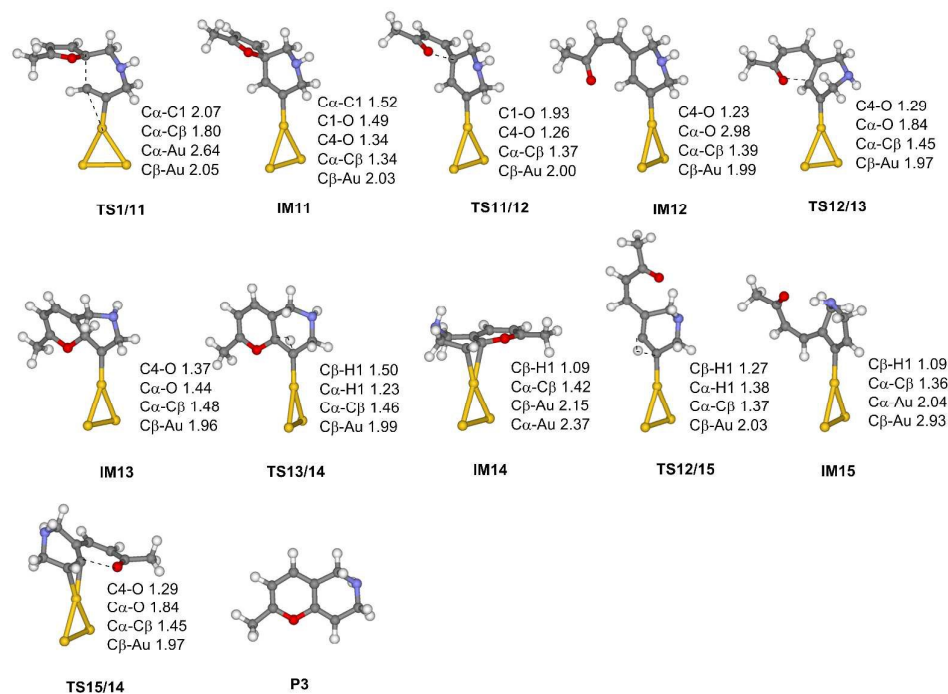


Fig. 5 The optimized structures and related parameters for the 6-endo FCT pathway toward pyran derivative **P3** (bond length in Å).

Journal Name

ARTICLE

Next, the oxygen atom of the C4=O bond attacks on the Au-C α bond to form a gold-oxepine complex **IM4** (the ring-closing of the dienone carbene-gold intermediate). This step is exothermic by about 10.35 and 1.05 kcal/mol with energy barriers of 12.22 and 16.99 kcal/mol in the gas phase and acetonitrile solvent, respectively. Finally, the oxepin derivative **IM5** is desorbed from the Au₃ cluster, which is endothermic by about 31.35 and 27.99 kcal/mol in the gas phase and acetonitrile, respectively. The benzene oxide **IM6** and the oxepin derivative **IM5** are in a tautomeric equilibrium during the reaction with an energy barrier of 5.42 (4.64) kcal/mol in the gas phase (acetonitrile). Finally, **IM6** is quickly converted into product phenols with an exothermicity of 39.44 (40.21) kcal/mol with heating or acid.^{1,2,17} Of note, the benzene oxide **IM6** was captured via a Diels-Alder reaction with dienophiles.¹⁷ In summary, the rate-limiting step of the 5-*exo* FCT reaction route is the nucleophilic addition of the C β atom to the C1 site of the furan ring to form the spiro-intermediate **IM2** with an energy barrier of 19.06 kcal/mol in the gas phase—the formation of the gold-oxepine complex **IM4** is the rate-determining step in acetonitrile.

In order to further prove the reasonability of the functional and basis set used in this paper, the 5-*exo* FCT pathway was calculated at the PBE/def2-TZVP levels. The calculated results are shown and summarized in Fig. S2 and Table S1. As shown in Figs. 1 and S2, the geometric parameters of the related structures with the TPSSh and PBE functionals are very similar. The adsorption energies of substrate, and energy barriers, and the reaction energies at the TPSSh/def2-TZVP and PBE/def2-TZVP levels are similar. Therefore, results with the TPSSh functional and def2-TZVP are reliable for the gold cluster-catalyzed the ω -alkynylfuran cycloisomerization.

We next focus on the pathway initializing from the [4+2] cycloaddition between the C α =C β bond and C1=C2-C3=C4 of furan ring in **IM1**, i.e. the DDA pathway (Figs. 2 and 3). The Diels-Alder adduct **IM7** (Fig. 2) has higher energy than **IM1** (2.54/2.12 kcal/mol in the gas phase/acetonitrile). The corresponding transition state **TS1/7** must overcome an energy barrier of 25.32 (26.24) kcal/mol in the gas phase (acetonitrile). The C α and C β atoms in **IM7** are approximately pyramidal, and the structure resembles a η^2 -gold-ene complex. Next, the bridged O atom would shift to the C α atom in **IM7** along with the breakage of the C1-O bond to form a gold-benzene oxide complex **IM8**. This step must overcome an energy barrier of 32.44 (25.44) kcal/mol in the gas phase (acetonitrile). Due to migration of the double bond from the C α -C β bond to the C1-C β bond in the process of **IM7** \rightarrow **IM8**, the interaction between the Au₃ cluster and the benzene oxide is very weak as reflected by the bond

length of the Au-C α and Au-C β bonds (Fig. 3). The weak interaction also results in the endothermicity of **IM7** \rightarrow **IM8**. Finally, the decomposition of **IM8** gives a Au₃ cluster and benzene oxide with slight endothermicity. Clearly, the migration of the bridged O atom step (**IM7** \rightarrow **IM8**) is the rate-limiting step for the DDA pathway with an energy barrier of 32.44 (25.44) kcal/mol in the gas phase (acetonitrile).

Finally, the pathway via the Au-vinylidene carbenoid complex (VDA pathway) (Figs. 2 and 3) was investigated. The gold-vinylidene carbenoid complexes are highly reactive intermediates—they are the key intermediate for many gold-catalyzed organic reactions.⁵¹⁻⁵⁷ The formation of Au-vinylidene carbenoid intermediate **IM9** is endothermic by about 10.06 (7.98) kcal/mol with an energy barrier of 44.95 (41.12) in the gas phase (acetonitrile). Obviously, the formation of the Au-vinylidene carbenoid intermediate **IM9** is unfavorable thermodynamically and kinetically, which agrees with the experimental findings.¹⁶ After the formation of the Au-vinylidene carbenoid intermediate **IM9**, the Diels-Alder adduct **IM10** is produced with an energy barrier of 28.43 (30.20) kcal/mol in the gas phase (acetonitrile). Due to the high ring tension, the Diels-Alder process (**IM9** \rightarrow **IM10**) is endothermic. Subsequently, the hydrogen atom on the C β atom transfers to the C α atom in **IM10** to give rise to **IM7**. The activation energy is predicted to be 29.79 (29.65) kcal/mol in the gas phase (acetonitrile). The remaining steps toward benzene oxide **IM6** are the same as that of the DDA pathway. The rate-limiting step of the VDA pathway is the formation of a Au-vinylidene carbenoid intermediate via the hydrogen transfer with an activation energy of 44.95 (41.12) in the gas phase (acetonitrile). Hence, this step is also unfavorable kinetically.

In summary, these findings indicate that the ω -alkynylfuran cycloisomerization to phenol catalyzed by a Au₃ cluster mainly proceeds via the 5-*exo* FCT pathway. All stationary points for the 5-*exo* FCT pathway stand below the separated catalyst and reactant, hence, the 5-*exo* FCT pathway proceeds easily. The rate-limiting step of the 5-*exo* FCT pathway is the first step, i.e. the 5-*exo* nucleophilic addition of C β atom to furan ring (**IM1** \rightarrow **IM2**). This point is highlighted by the fact that no intermediate could be detected in the experiments, which concurs with the experimental data.¹⁷ The formation of Diels-Alder adduct **IM7** and Au-vinylidene carbenoid intermediate **IM9** are both thermodynamically and kinetically unfavorable.

Pathways for the formation of pyran derivative. There is a 6-*endo* FCT pathways, i.e., the nucleophilic addition of a C α atom to the furan ring in **IM1**, which is in competition with the 5-*exo* FCT pathway. The 6-*endo* FCT pathway finally leads to a pyran

derivative. The optimized structures, related parameters, and potential energy profiles are shown in Figs. 4 and 5.

The 6-*endo* nucleophilic addition of C α atom to the C1 atom of the furan ring in **IM1** results in a metastable spiro intermediate **IM11** via **TS1/11**. The predicted activation energy is 20.19 (18.94) kcal/mol in the gas phase (acetonitrile), which is slightly higher than that of formation in the 5-*exo* nucleophilic addition intermediate **IM2**. Subsequently, cleavage of the C1-O bond of the furan ring in **IM11** produces intermediate **IM12**—the C4-O single bond changes to a C4-O double bond. This process requires an energy barrier of 7.29 (7.20) kcal/mol with an exothermicity of 8.16 (12.53) kcal/mol in the gas phase (acetonitrile).

Next, there are two pathways from **IM12** to the final product **P3**. The first pathway is via the O atom of the C4=O bond that attacks the C α atom to result in the six-membered ring intermediate **IM13**. Then, the H atom on the C α atom migrates to the C β atom to generate product complex **IM14**. The corresponding energy barriers are 23.97 (29.26) (**IM12** \rightarrow **IM13**) and 6.37 (6.88) (**IM13** \rightarrow **IM14**) kcal/mol in the gas phase (acetonitrile).

Alternately, the migration of the H atom from the C α atom to the C β atom overcomes an energy barrier of 55.48 (60.56) kcal/mol to produce intermediate **IM15**. Subsequently, the carbonyl group nucleophilically attacks the C α atom to result in product complex **IM14**. The activation energy is only 9.76 (17.65) kcal/mol (**TS15/14**) with an exothermicity of 27.89 (17.91) kcal/mol. Comparison of the two hydrogen steps (**IM12** \rightarrow **IM15** and **IM13** \rightarrow **IM14**) shows that the higher energy barriers of **IM12** \rightarrow **IM15** are ascribed to the strong C(sp²)-H bond in **IM12**. Simultaneously, the electron-deficient C α atom in **IM15** results in a low energy barrier of **TS15/14**. Finally, the pyran derivative **P3** is desorbed from **IM14** with regeneration of Au₃ cluster, which is endothermic by 31.21 (28.08) kcal/mol in the gas phase (acetonitrile). Obviously, the energy barriers of formation for the pyran derivative are higher than that of the 5-*exo* FCT pathway.

The pathway for the formation of the β -alkenylated furan (**P2**) has also been studied. However, only the minimum of **11** was located. The transition state connecting **IM1** and **11** could not be obtained with our best efforts. At the same time, the transition states of the C β migration from the C1 atom to the C2 atom (**IM2** \rightarrow **11**) as well as the gold-cyclopropylcarbene complex to **11** could not be located. The charges on the C1 and C2 atoms of the furan ring in **IM1** are 0.23 and -0.29 |e|, respectively. Hence, the C α atom could preferably attack the C1 atom to form **IM2**. Therefore, the formation of β -alkenylated furan is not favorable for the ω -alkynylfuran cycloisomerization catalyzed by Au₃ cluster.

To better understand the 5-*exo* FCT pathway, DDA pathway, and 6-*endo* FCT pathway, we performed energy decomposition analysis (EDA)^{22,23,58-60} on the energy barriers and reaction energy for the first steps of the three pathways (**IM1** \rightarrow **IM2**,

Table 1. Energy barriers ($\Delta_r E_a$) and their energy components for the three competitive pathways catalyzed by the Au₃ cluster (units in kcal/mol).

Reactions	$\Delta E_{\text{int-1}}$	$\Delta E_{\text{int-2}}$	ΔE_{B}	$\Delta E_{\text{D-Sub}}$	$\Delta E_{\text{D-Ca}}$	$\Delta_r E_a / \Delta_r E$
IM1 \rightarrow TS1/2	-45.92	-49.49	-3.57	23.20	-0.04	19.59
IM1 \rightarrow TS1/7	-45.92	-50.36	-4.44	29.93	0.07	25.56
IM1 \rightarrow TS1/11	-45.92	-48.20	-2.28	22.95	0.02	20.69
IM1 \rightarrow IM2	-45.92	-82.84	-36.92	44.31	-0.64	6.75
IM1 \rightarrow IM7	-45.92	-51.26	-5.34	6.06	0.07	0.79
IM1 \rightarrow IM11	-45.92	-76.68	-30.76	35.26	-0.65	3.85

IM1 \rightarrow **IM7**, and **IM1** \rightarrow **IM11**). The details of the EDA were supplied in the Supporting Information. Concisely, the energy barriers and reaction energies are decomposed into three parts. The first part is the deformation (distortion) energies of substrate fragment (Sub) from reactants to transition states (products). The second part is the deformation (distortion) energies of catalyst fragment (Au₃, Ca) from reactants to transition states (products). The last part is the change in interaction energy (ΔE_{b}) between the Sub and Ca fragments from reactants to transition states or products. The EDA results are shown in Table 1 and indicate that the deformation energies of the Au₃ fragments for these processes are very small suggesting only small structural changes in the Au₃ fragments. The changes in binding energies are slightly favorable for the three pathways. The energy barriers are mainly due to the deformation of the Sub fragments. Simultaneously, the differences in energy barriers of the three pathways originate from the structural deformation of a Sub fragment. The changes in binding energies between Au₃ and Sub fragments counteract the deformation energies of the Sub fragments in **IM2** and **IM7**. Therefore, the strong interaction between gold and vinyl in Friedel-Crafts adduct stabilizes the Friedel-Crafts addition intermediates. This results in high selectivity toward the phenol derivative.

Size-effect of planar gold clusters

Oliver-Meseguer et al. found the Au₃₋₁₀ clusters were formed in reaction progress. Simultaneously, the various-sized gold clusters showed different catalytic activity for alkyne activation reactions.¹⁸⁻²¹ Therefore, the mechanism on Au₄₋₁₀ clusters were investigated to illustrate the catalytic activity of the planar gold clusters toward the ω -alkynylfuran cycloisomerization. Because our goal is to explore the reaction activity of neutral planar gold clusters, compared with that of Au₃ and Au₄ clusters. Therefore, although many reports show the structures (both 2D and 3D) of bigger clusters are closely related to the calculation methods,^{49,61,62} the relatively stable planar structures of Au₅₋₁₀ clusters are chosen in the present article (Fig. 6). At the same time, as shown in Fig. S1, the most stable structures of Au₃₋₁₀ are planar at the TPSSh/def2-TZVP level. From

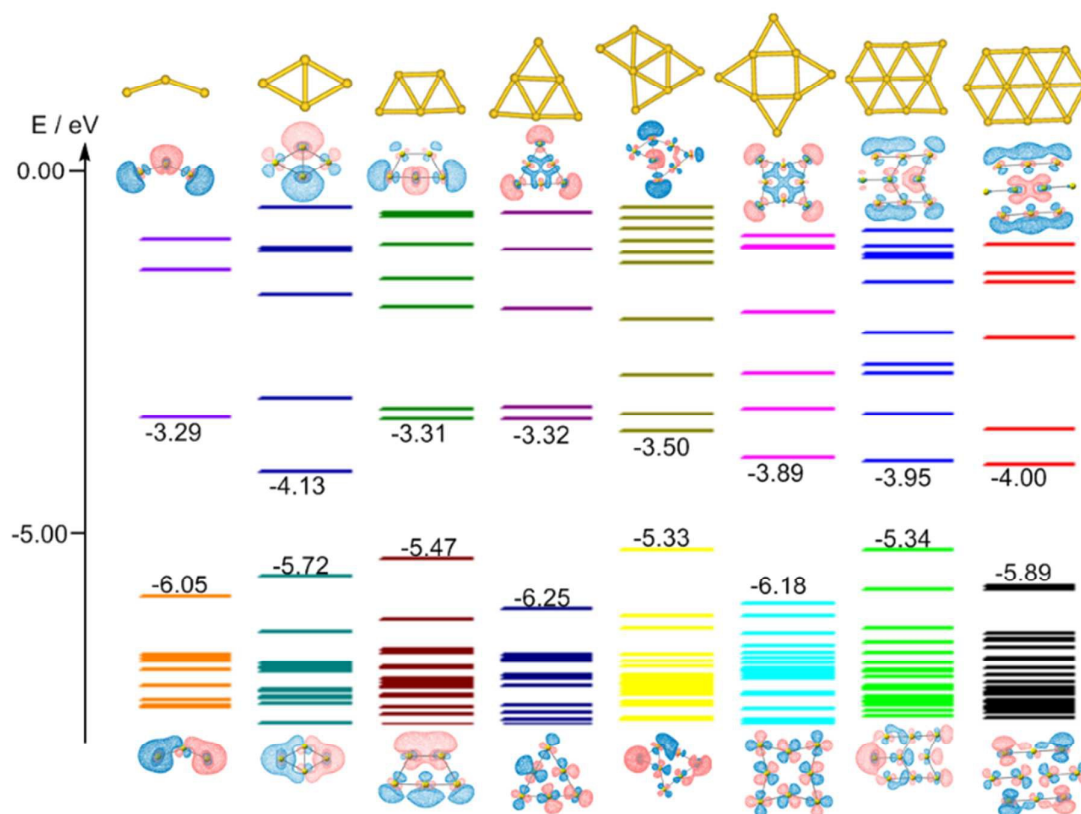


Fig. 6. The structures and isosurfaces (cutoff = 0.03) of the HOMO and LUMO orbitals of the planar gold clusters.

above discussions on Au_3 cluster-catalyzed ω -alkynylfuran cycloisomerization, the 5-*exo* FCT mechanism was the most favorable mechanism to synthesize phenol. So, only the 5-*exo* FCT mechanism on Au_{4-10} clusters were studied. The energy profiles, optimized structures, and related parameters are shown in Figs. S3-S9. The **TS3/4** of Au_6 cluster was not located in this study. The relaxed scan along the $\text{C}\alpha\text{-O}$ bond (Fig. S10) showed no energetic maximum between **IM3** and **IM4** for Au_6 cluster. The relaxed scan of potential energy profile for **TS3/4** in the Au_8 cluster was also performed (Fig. S10).

Firstly, the adsorption of ω -alkynylfuran on these clusters was analyzed. The adsorption energy of ω -alkynylfuran on the Au_4 cluster is -33.58 and -29.64 kcal/mol in the gas phase and acetonitrile solvent, respectively. This is comparable to that of the Au_3 cluster (-32.84 and -29.05 kcal/mol). It is interesting that the ω -alkynylfuran is preferentially adsorbed on the acute vertex of the

Au_4 cluster. To confirm this point, the isosurface of the highest occupied molecular orbital (HOMO) and lowest occupied molecular orbital (LUMO) of the Au_4 cluster were drawn (Fig. 6). Fig. 6 highlights that the main contribution of the LUMO is the acute vertex of the Au_4 cluster, which agrees with the adsorption of the substrate.

The adsorption energies of the ω -alkynylfuran on the Au_{5-10} clusters are in the range of -21 to -16 kcal/mol (Table 2). These results suggest that ω -alkynylfuran is more favorably adsorbed on the Au_3 and Au_4 clusters than on other planar gold clusters ($\text{Au}_5\text{-Au}_{10}$). The higher adsorption energies on the Au_3 and Au_4 clusters could be attributed to the large back-donation from the d orbital of the gold atom to the π^* orbital of the $\text{C}\alpha\equiv\text{C}\beta$ bond. The different back-donation could be characterized by the different bond lengths of the $\text{C}\alpha\equiv\text{C}\beta$ bond. The binding strength of the substrate with gold is controlled by the degree of charge transfer and two different

Table 2. The adsorption energies (ΔE_{ad} , kcal/mol) of substrate on the gold clusters (GC) and the energy barriers (ΔE_a , kcal/mol) of three steps in the gas phase and acetonitrile solvent (parentheses).

GC	ΔE_{ad}	$\Delta E_a(\text{TS1/2})$	$\Delta E_a(\text{TS2/3})$	$\Delta E_a(\text{TS3/4})$
Au ₃	-32.84(-29.05)	19.06(15.87)	8.48(8.44)	12.21(16.99)
Au ₄	-33.58(-29.64)	19.92(16.92)	2.57(1.37)	6.81(5.48)
Au ₅	-21.11(-18.48)	13.86(13.59)	13.43(13.72)	13.42(14.36)
Au ₆	-16.55(-12.81)	11.61(12.23)	8.14(5.48)	-
Au ₇	-16.15(-13.16)	9.14(8.79)	11.68(12.22)	13.92(15.08)
Au ₈	-19.66(-15.58)	14.35(11.60)	6.44(4.60)	3.92(2.99)
Au ₉	-18.54(-14.94)	12.01(10.88)	8.90(5.53)	12.68(19.55)
Au ₁₀	-16.83(-14.32)	13.94(13.18)	6.97(4.28)	4.49(4.74)

electron density transfer processes: σ -donation from the alkyne fragment to the gold and π -back-donation from the gold to the alkyne fragment. Therefore, the strength of the interaction depends on two factors: the difference in energy and the spatial overlap between the orbitals involved. The HOMO and LUMO orbitals of planar gold clusters consist of several lobes (Fig. 6). These are mainly localized on the edge and corner gold atoms and are fully accessible to interaction with the alkyne fragments of the substrate. This efficient overlap between the molecular orbitals explains the higher adsorption energy values and the preferred adsorption sites.

The energy barriers of the 5-*exo* cyclization step are from 9.00 to 14.50 kcal/mol for Au₅₋₁₀ clusters in the gas phase. Those for Au₃ and Au₄ clusters are 19.00 kcal/mol. Analysis of the energy barriers of the 5-*exo* cyclization step and the adsorption energies of the substrate showed that large adsorption energies result in high energy barriers for the 5-*exo* cyclization step. This point should be attributed to the decreasing interaction between the C β atom of substrate fragment and gold clusters in during the 5-*exo* cyclization step. Hence, the appropriate interactions between the substrate and gold clusters are essential for the 5-*exo* cyclization step. These findings are also supported by the EDA results (Tables S1-S8). The ring-opening of the furan step on the Au₄₋₁₀ clusters is exothermic with moderate energy barriers (Table 2).

The energy barriers of the ring-closing of the dienone carbene-gold step show an interesting "odd-even" behavior respective to the number of gold atoms. Indeed, the energy barriers on odd-numbered gold clusters (Au₅, Au₇, Au₉) are commonly higher than that on gold clusters with even-numbered atoms (Au₆, Au₈, Au₁₀; Table 2). The different energy barriers on Au₃₋₁₀ clusters are ascribed to that of the gold clusters with odd numbers of electrons that can strongly bind with the carbene fragment in **IM3**. Table 2 shows that the rate-determining step is the 5-*exo* cyclization step

on an even-numbered gold clusters, while the rate-limiting step is the ring-closing of dienone carbene-gold intermediate step (**IM3**→**IM4**) with odd-numbered gold clusters as catalysts. This is attributed to the strong interactions between the gold atom and the carbene fragment for the odd-numbered gold clusters as catalysts. The length of the Au-C α bond in Figs. S3-S9 could not determine this interaction difference. To confirm these findings, we performed EDA on the ring-closing of the dienone carbene-gold intermediate step (**IM3**→**IM4**). As shown in Tables S2-S9, the interaction energies between the gold clusters and the carbene fragment in **IM3** of the odd-numbered gold clusters are larger than those of even-numbered gold clusters. This results in a stronger Au-C α bond in the odd-numbered gold clusters. The ring-closing of the dienone carbene-gold intermediate step involves the nonequivalent hybridization sp² orbital of the O atom interaction with the π orbital of the Au=C α bond to form a C α -O bond, which weakens the Au-C α bond. Therefore, the strong Au-C α bond of the odd-numbered gold clusters results in large energy barriers.

As shown in Figs. S3-S9, all of the energy profiles suggest that the planar gold clusters have good catalytic activity toward the ω -alkynylfuran cycloisomerization to the phenol derivative. However, the free energy profiles at 298.15 K and 1 atm indicate that the ω -alkynylfuran cycloisomerization to phenol derivative catalyzed by Au₅₋₁₀ clusters must overcome energy barriers of about 5.00 - 18.56 kcal/mol. Hence, Au₃ and Au₄ clusters show better catalytic activity toward the ω -alkynylfuran cycloisomerization to phenol derivative than that of Au₅₋₁₀ clusters at experimental conditions. This is in line with experimental results.¹⁸

Comparison with Gold(I) Complexes

To distinguish the difference between the gold clusters and gold complexes-catalyzed ω -alkynylfuran cycloisomerization, the possible reaction pathways of the ω -alkynylfuran cycloisomerization catalyzed by the [AuP(CH₃)₃]⁺ complex was investigated. The reactions were taken from refs 4 and 10. The P(CH₃)₃ was used to model the PPh₃ to reduce the computational times. The optimized structures, related parameters, potential energy profiles, and relative Gibbs free energies were shown in Figs. S11 and S12. It was should be noted that the 5-*exo* FCT pathway toward the phenol derivative **P1** and the pathway toward the pyran derivative **P3** could be not obtained with our efforts. Simultaneously, the VDA pathway was not considered due to the high barriers of the formation of the gold-vinylidene carbenoid intermediate. Only the DDA pathway toward the phenol derivative **P1** and the 6-*endo* nucleophilic

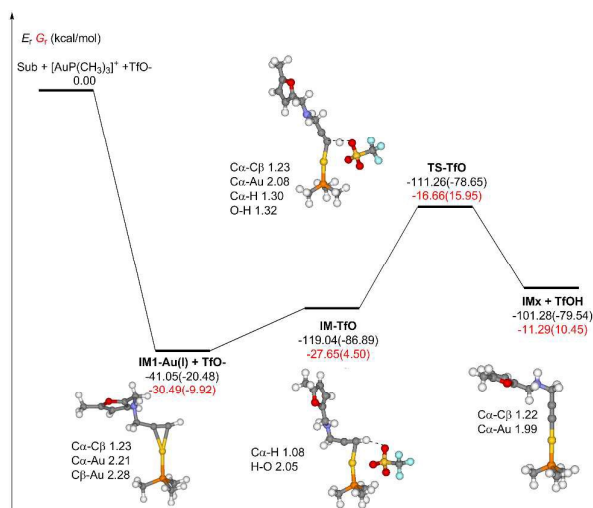


Fig. 7. The optimized structures, related parameters, potential energy profile, and relative Gibbs free energies (colored by red, 298.15 K and 1 atm) of the transfer of the terminal hydrogen of the alkyne group to TfO⁻ in the gas phase and acetonitrile solvent (parentheses). The bond length is in Å.

pathway toward the β -alkenylated furan (**P2**) were shown in Figs. S11 and S12.

As shown in Fig. S11, the coordination of the ω -alkynylfuran with the [AuP(CH₃)₃]⁺ complex is exothermic by about 41.05(20.48) kcal/mol in the gas phase (acetonitrile). The orbital interaction between the alkynyl group and the gold(I) complex are mainly the donation of the electron from the π orbital of the alkynyl group to the unoccupied d orbitals of the gold atom and the back-donation of the electron from the occupied d orbitals of the gold atom to the π^* orbital of the alkynyl group. The intramolecular addition of the C \equiv C triple bond to the furan ring in **IM1-Au(I)** slightly endothermic due to the deformation of the aromaticity of the furan ring. The energy barrier is 24.01(26.47) kcal/mol in the gas phase (acetonitrile). Obviously, this step is unfeasible kinetically. Next, the bridged O atom would migrate to the C α atom in **IM2-Au(I)** along with the breakage of the C1-O bond to form a gold-benzene oxide complex **IM3-Au(I)**. Due to the twist of the six-membered ring, this step also need overran an energy barrier of 20.91(26.08) kcal/mol in the gas phase (acetonitrile). Finally, the decomposition of **IM3-Au(I)** is endothermic by about 16 kcal/mol in acetonitrile. After consideration of the entropy effect, this step is only endothermicity of 5.27 kcal/mol in acetonitrile. The whole reaction pathway need overcome a free energy barrier of 29.81 kcal/mol in acetonitrile at 298.15 K.

The pathway of the formation of the β -alkenylated furan (**P2**) is initialized from the nucleophilic addition of the C β atom to the C1 site of the furan ring to produce a spiro-intermediate **IM4-Au(I)** (the 5-*exo* cyclization step). This step is slightly exothermic with an energy barrier of 3.54(8.46) kcal/mol in the gas phase (acetonitrile). It should be noted that the pathway toward the phenol derivative **P1** from **IM4-Au(I)** could not be obtained. The relaxed scan of the potential energy profiles at the TPSSH/def2-TZVP levels could not

obtain the pathway. Next, the migration of the C β atom from the C1 atom to the C2 atom produce **IM5-Au(I)** with an energy barrier of 10.56(13.09) kcal/mol in the gas phase (acetonitrile). This step is endothermic by about 10 kcal/mol because of the repulsion between the C2 and C β atoms in **IM5-Au(I)**, which is also certified by the long C2-C β bond in **IM5-Au(I)**. Then, the hydrogen atom on the C2 atom transfers to the C β atom via a four-membered ring transition state **TS5/6-Au(I)**. This step is the rate-limiting step of this pathway with an energy barrier of 14.45(15.40) kcal/mol in the gas phase (acetonitrile). Finally, the β -alkenylated furan (**P2**) is detached from **IM6-Au(I)** with an endothermicity of 10 kcal/mol in acetonitrile.

Obviously, the feasible pathway of the ω -alkynylfuran cycloisomerization catalyzed by the [AuP(CH₃)₃]⁺ complex is the formation of the β -alkenylated furan (**P2**), which is not in line with the production distribution of the experiments.²⁻¹² The main product of the ω -alkynylfuran cycloisomerization catalyzed by the [AuP(CH₃)₃]⁺ complex should be the phenol derivative **P1**. To solve this problem, we further consider the reduction of the [AuP(CH₃)₃]⁺ complex to AuP(CH₃)₃ by the terminal alkyne. As shown in Fig. 7, the transfer of the terminal hydrogen of the alkyne group to TfO⁻ (CF₃SO₃⁻) was studied. Obviously, the formation of the **IM-TfO** intermediate should be exothermic due to the strong electrostatic interaction and hydrogen bond, while the change of the free energy in the acetonitrile solvent due to the decrease of the entropy. The hydrogen transfer step must overwhelm an energy barrier of about 10 kcal/mol to produce **IMx** and TfOH. The reduction of the [AuP(CH₃)₃]⁺ complex to AuP(CH₃)₃ by the terminal alkyne need overrun 16 kcal/mol of free energy barrier in acetonitrile. Hence, the [AuP(CH₃)₃]⁺ complex could be reduced to AuP(CH₃)₃ *in situ* by the terminal alkyne. Therefore, all of the possible pathways of the ω -alkynylfuran cycloisomerization catalyzed by AuP(CH₃)₃ were studied. The optimized structures, related parameters, potential energy profiles, and relative Gibbs free energies were shown in Figs. S13-S15. It is similar with that of the Au₃ cluster; the pathway for the formation of the β -alkenylated furan (**P2**) is not obtained. As shown in Fig. S13, the energy barrier of the rate-limiting step of the 5-*exo* FCT pathway catalyzed by AuP(CH₃)₃ is 14.90(15.23) kcal/mol. Simultaneously, the DDA pathway need to overcome an energy barrier of 19.44(20.82) kcal/mol. The pathway of the formation of the pyran derivative must surmount an energy barrier of 25.96(27.61) kcal/mol. Hence, the most feasible pathway of the ω -alkynylfuran cycloisomerization catalyzed by AuP(CH₃)₃ is the 5-*exo* FCT pathway with the formation of the phenol derivative. After incorporation of the reduction of [AuP(CH₃)₃]⁺ complex to AuP(CH₃)₃, the free energy barrier of the 5-*exo* FCT pathway is about 16 kcal/mol in acetonitrile.

Comparison of the potential energy and the free energy profiles in Figs. S11-S15, it is found that the 5-*exo* FCT pathway catalyzed by AuP(CH₃)₃ is the most feasible pathway thermodynamically and kinetically. Then, the pathway of the formation of the β -alkenylated furan (**P2**) by [AuP(CH₃)₃]⁺ is

feasible kinetically, however, the whole pathway must overcome about 17.08 kcal/mol of free energy barrier at 298.15 K. Therefore, we can conclude that the active catalyst for the ω -alkynylfuran cycloisomerization is the reduction state of the $[\text{AuP}(\text{CH}_3)_3]^+$ complex, *i.e.* $\text{AuP}(\text{CH}_3)_3$. The byproduct (the β -alkenylated furan) is produced from the cyclization of the ω -alkynylfuran catalyzed by the $[\text{AuP}(\text{CH}_3)_3]^+$ complex. The selectivity is mainly controlled by the steric effect of the ligand and the polarity of the solvent. The product distribution is in line with the experiments.¹⁰ The catalytic activity of the gold(0) complex is comparable with that of the planar gold clusters.

Conclusions

In summary, the full mechanism of the ω -alkynylfuran cycloisomerization catalyzed by a Au_3 cluster was investigated at the TPSSH/def2-TZVP levels. Four pathways were identified and analyzed. The 5-*exo* Friedel-Crafts-type mechanism is the most favorable pathway to produce a phenol derivative with an energy barrier of 19.06 (16.99) kcal/mol in the gas phase (acetonitrile). The 6-*endo* FCT, DDA, and VDA pathways are unfavorable due to the high-energy barriers of the hydrogen migration steps. The strong interaction between gold and vinyl in the Friedel-Crafts adduct stabilizes the Friedel-Crafts addition intermediates. The 5-*exo* FCT pathways on the planar gold clusters (Au_{3-10}) were studied to clarify the effect size. The appropriate interactions between the substrate and gold clusters are essential for the 5-*exo* cyclization step. The energy barriers of the ring-closing of the dienone carbene-gold intermediate step show an interesting "odd-even" behavior respective to the number of gold atoms. The Au_3 and Au_4 clusters show better catalytic activity toward the ω -alkynylfuran cycloisomerization to phenol derivative than the Au_{5-10} clusters under experimental conditions—this was again confirmed with experimental data. The trade-off studies show that the active catalyst of the ω -alkynylfuran cycloisomerization catalyzed by the gold(I) complexes should be the gold(0) complexes, which is forming *in situ* reduction by the ω -alkynylfuran. The catalytic activity of the gold(0) complex is comparable with that of the planar gold clusters.

Acknowledgements

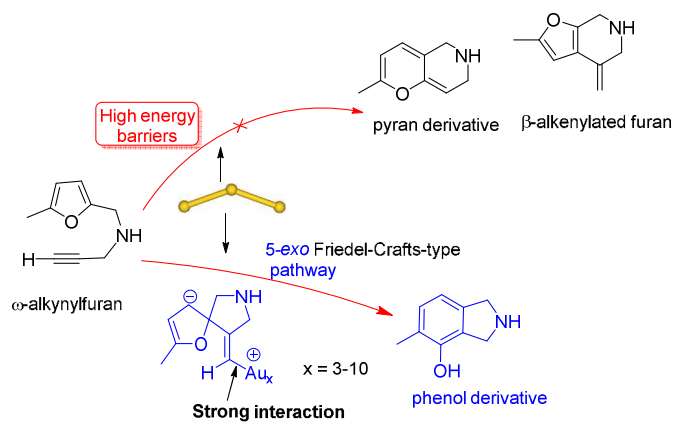
This work was supported by the National Natural Science Foundation of China (Grant No. 21573030), the Chongqing Science & Technology Commission, China (Grant No. CSTC2013JCYJA50028) and the Scientific Research Foundation of Chongqing University of Arts and Sciences (R2013CJ03). The calculations were performed at the National Supercomputing Center in Shenzhen (Shenzhen Cloud Computing Center).

Notes and references

- A. S. K. Hashmi, T. M. Frost and J. W. Bats, *J. Am. Chem. Soc.*, 2000, **122**, 11553-11554.
- A. S. K. Hashmi, T. M. Frost and J. W. Bats, *Org. Lett.*, 2001, **3**, 3769-3771.
- A. S. K. Hashmi, J. P. Weyrauch, M. Rudolph and E. Kurpejovic, *Angew. Chem. Int. Ed.*, 2004, **43**, 6545-6547.
- A. S. K. Hashmi, M. C. Blanco, E. Kurpejovic, W. Frey and J. W. Bats, *Adv. Synth. Catal.*, 2006, **348**, 709-713.
- A. S. K. Hashmi, R. Salathe and W. Frey, *Chem. Eur. J.*, 2006, **12**, 6991-6996.
- A. S. K. Hashmi, J. P. Weyrauch, E. Kurpejovic, T. M. Frost, B.; Frey, W. Miehlich and J. W. Bats, *Chem. Eur. J.*, 2006, **12**, 5806-5814.
- A. S. K. Hashmi, E. Kurpejovic, M. Wolffe, W. Frey and J. W. Bats, *Adv. Synth. Catal.*, 2007, **349**, 1743-1750.
- A. S. K. Hashmi, M. Rudolph, J. W. Bats, W. Frey, F. Rominger and T. Oeser, *Chem. Eur. J.*, 2008, **14**, 6672-6678.
- Y. Chen, W. Yan, N. G. Akhmedov and X. Shi, *Org. Lett.*, 2010, **12**, 344-347.
- A. S. K. Hashmi, J. Hofmann, S. Shi, A. Schutz, M. Rudolph, C. Lothschutz, M. Wietek, M. Buhrle, M. Wolffe and F. Rominger, *Chem. Eur. J.*, 2013, **19**, 382-389.
- M. C. B. Jaimes, C. R. N. Bohling, J. M. Serrano-Becerra and A. S. K. Hashmi, *Angew. Chem. Int. Ed.*, 2013, **52**, 7963-7966.
- M. C. B. Jaimes, F. Rominger, M. M. Pereira, R. M. B. Carrilho, S. A. C. Carabineiro and A. S. K. Hashmi, *Chem. Commun.*, 2014, **50**, 4937-4940.
- B. Martin-Matute, D. J. Cardenas and A. M. Echavarren, *Angew. Chem. Int. Ed.*, 2001, **40**, 4754-4757.
- B. Martin-Matute, C. Nevado, D. J. Cardenas and A. M. Echavarren, *J. Am. Chem. Soc.*, 2003, **125**, 5757-5766.
- S. Carrettin, M. C. Blanco, A. Corma and A. S. K. Hashmi, *Adv. Synth. Catal.*, 2006, **348**, 1283-1288.
- A. S. K. Hashmi, M. Rudolph, H.-U. Siehl, M. Tanaka, J. W. Bats and W. Frey, *Chem. Eur. J.*, 2008, **14**, 3703-3708.
- A. S. K. Hashmi, M. Rudolph, J. P. Weyrauch, M. Wolffe, W. Frey and J. W. Bats, *Angew. Chem. Int. Ed.*, 2005, **44**, 2798-2801.
- J. Oliver-Meseguer, A. Leyva-Perez and A. Corma, *ChemCatChem.*, 2013, **5**, 3509-3515.
- J. Oliver-Meseguer, J. R. Cabrero-Antonino, I. Dominguez, A. Leyva-Perez and A. Corma, *Science*, 2012, **338**, 1452-1455.
- A. S. K. Hashmi, *Science*, 2012, **338**, 1434-1434.
- J. Oliver-Meseguer, A. Leyva-Perez, S. I. Al-Resayes and A. Corma, *Chem. Commun.*, 2013, **49**, 7782-7784.
- D. Tang, Z. Chen, Y. Tang, J. Zhang, Z. Xu and J. Zhang, *J. Phys. Chem. C*, 2014, **118**, 18510-18520.
- D. Tang, Z. Chen, J. Zhang, Y. Tang and Z. Xu, *Organometallics*, 2014, **33**, 6633-6642.
- J. M. Tao, J. P. Perdew, V. N. Staroverov and G. E. Scuseria, *Phys. Rev. Lett.*, 2003, **91**, 146401/1-4.
- K. P. Jensen, *Inorg. Chem.*, 2008, **47**, 10357-10365.
- F. Weigend and R. Ahlrichs, *Phys. Chem. Chem. Phys.*, 2005, **7**, 3297-3305.
- M. J. Frisch, G. W. Trucks, H. B. Schlegel, G. E. Scuseria, M. A. Robb, J. R. Cheeseman, G. Scalmani, V. Barone, B. Mennucci, G. A. Petersson, et al. Gaussian 09, Revision D.01; Gaussian, Inc., Wallingford, CT, 2009.
- H. P. Hratchian and H. B. Schlegel, *J. Chem. Phys.*, 2004, **120**, 9918-9924.
- H. P. Hratchian and H. B. Schlegel, *J. Chem. Theory Comput.*, 2005, **1**, 61-69.
- A. V. Marenich, C. J. Cramer and D. G. Truhlar, *J. Phys. Chem. B*, 2009, **113**, 6378-6396.
- Y.-K. Shi, Z. H. Li and K.-N. Fan, *J. Phys. Chem. A*, 2010, **114**, 10297-10308.
- L. Li, Y. Gao, H. Li, Y. Zhao, Y. Pei, Z. Chen and X. C. Zeng, *J. Am. Chem. Soc.* 2013, **135**, 19336-19346.
- C. Liu, Y. Tan, S. Lin, H. Li, X. Wu, L. Li, Y. Pei and X. C. Zeng, *J. Am. Chem. Soc.*, 2013, **135**, 2583-2595.
- S. Lin and Y. Pei, *J. Phys. Chem. C*, 2014, **118**, 20346-20356.

- 35 M. Boronat, T. López-Ausens and A. Corma, *J. Phys. Chem. C*, 2014, **118**, 9018-9029.
- 36 R.-J. Lin, H.-L. Chen, S.-P. Ju, F.Y. Li and H.-T. Chen, *J. Phys. Chem. C*, 2012, **116**, 336-342.
- 37 Y. Zhao, D. G. and Truhlar, *Theor. Chem. Acc.*, 2008, **120**, 215-241.
- 38 Y. Zhao and D. G. Truhlar, *J. Chem. Phys.*, 2006, **125**, 194101/1-18.
- 39 N. E. Schultz, Y. Zhao and D. G. Truhlar, *J. Phys. Chem. A* 2005, **109**, 11127-11143.
- 40 Y. Zhao, N. E. Schultz and D. G. Truhlar, *J. Chem. Theory Comput.* 2006, **2**, 364-382.
- 41 T. M. Soini, A. Genest, A. Nikodem and N. Rösch, *J. Chem. Theory Comput.* 2014, **10**, 4408-4416.
- 42 P. Janthon, S. Luo, S. M. Kozlov, F. Viñes, J. Limtrakul, D. G. Truhlar and F. Illas, *J. Chem. Theory Comput.* 2014, **10**, 3832-3839.
- 43 B. Chan and W.-L. Yim, *J. Chem. Theory Comput.* 2013, **9**, 1964-1970.
- 44 G. A. Bishea and M. D. Morse, *J. Chem. Phys.* 1991, **95**, 5646-5659.
- 45 A. M. James, P. Kowalczyk, B. Simard, J. C. Pinegar and M. D. Morse, *J. Mol. Spectrosc.* 1994, **168**, 248-257.
- 46 K. Hilpert and K. A. Gingerich, *Ber. Bunsen-Ges. Phys. Chem.*, 1980, **84**, 739-745.
- 47 B. Assadollahzadeha and P. Schwerdtfeger *J. Chem. Phys.*, 2009, **131**, 064306/1-11.
- 48 S. A. Serapian, M. J. Bearpark and F. Bresme, *Nanoscale*, 2013, **5**, 6445-6457.
- 49 M. P. Johansson, I. Warnke, A. Le and F. Furche, *J. Phys. Chem. C*, 2014, **118**, 29370-29377.
- 50 G. A. Bishea and M. D. Morse, *J. Chem. Phys.*, 1991, **95**, 8779-8792.
- 51 A. S. K. Hashmi, I. Braun, M. Rudolph and F. Rominger, *Organometallics*, 2012, **31**, 644-661.
- 52 A. S. K. Hashmi, M.; Wieteck, I. Braun, P. Nosel, L. Jongbloed, M. Rudolph and F. Rominger, *Adv. Synth. Catal.*, 2012, **354**, 555-562.
- 53 A. S. K. Hashmi, M.; Wieteck, I. Braun, M. Rudolph and F. Rominger, *Angew. Chem., Int. Ed.*, 2012, **51**, 10633-10637.
- 54 M. M. Hansmann, M. Rudolph, F. Rominger and A. S. K. Hashmi, *Angew. Chem., Int. Ed.*, 2013, **52**, 2593-2598.
- 55 M. H. Vilhelmsen and A. S. K. Hashmi, *Chem. Eur. J.*, 2014, **20**, 1901-1908.
- 56 J. Bucher, T. Wurm, K. S. Nalivela, M. Rudolph, F. Rominger and A. S. K. Hashmi, *Angew. Chem., Int. Ed.*, 2014, **53**, 3854-3858.
- 57 M. M. Hansmann, F. Rominger and A. S. K. Hashmi, *Chem. Sci.*, 2013, **04**, 1552-1559.
- 58 B. Hammer, *Surf. Sci.*, 2000, **459**, 323-348.
- 59 C. Dupont, Y. Jugnet and D. Loffreda, *J. Am. Chem. Soc.*, 2006, **128**, 9129-9136.
- 60 Z. Wei, D. Li, X. Pang, C. Lv and G. Wang, *ChemCatChem*, 2012, **4**, 100-111.
- 61 Y. C. Choi, W. Y. Kim, H. M. Lee, K. S. Kim, *J. Chem. Theory Comput.*, 2009, **5**, 1216-1223.
- 62 R. M. Olson, S. Varganov, M. S. Gordon, H. Metiu, S. Chretien, P. Piecuch, K. Kowalski, S. A. Kucharski and M. Musial, *J. Am. Chem. Soc.*, 2005, **127**, 1049-1052.

Graphical Abstract



A detailed reaction mechanism of Au_{3-10} -catalyzed cycloisomerization of ω -alkynylfuran was systemically investigated at the TPSSh/def2-TZVP levels.